Modeling sand wave characteristics on the Belgian Continental Shelf and in the Calais-Dover Strait

J. Cherlet,[1] G. Besio,[1] P. Blondeaux,[1] V. van Lancker,[2] E. Verfaillie,[2] and G. Vittori[1]

Received 8 January 2007; revised 16 March 2007; accepted 5 April 2007; published 1 June 2007.

[1] The capability of the model of Besio et al. (2006) to predict the main geometrical characteristics (crest orientation, wavelength,...) of tidal sand waves is tested by comparing the theoretical predictions with field data. In particular the field observations carried out by Mouchet (1990) and Van Lancker et al. (2005) along the continental shelf of Belgium are used. Additional comparisons are carried out against the field measurements described by Le Bot (2001) and Le Bot and Trenteseaux (2004) which were carried out in an adjacent region. Attention is focused on the prediction of the wavelength of the bottom forms. Indeed, the capability of a linear stability analysis to predict the occurrence of sand waves has been already tested by Hulscher and van den Brink (2001) and more recently by van der Veen et al. (2006). The obtained results show that the theoretical predictions fairly agree with field observations even though some of the comparisons suggest that the accuracy of the predictions depends on the accurate evaluation of the local current and sediment characteristics.

Citation: Cherlet, J., G. Besio, P. Blondeaux, V. van Lancker, E. Verfaillie, and G. Vittori (2007), Modeling sand wave characteristics on the Belgian Continental Shelf and in the Calais-Dover Strait, *J. Geophys. Res.*, *112*, C06002, doi:10.1029/2007JC004089.

1. Introduction

[2] In the coastal region, the interaction of the flow generated by waves and currents with the cohesionless sea bottom gives rise to a variety of bottom forms characterized by length scales falling in a wide range. The smallest sedimentary structures are called ripples [*Allen*, 1984; *Sleath*, 1984] which can be generated either by steady currents [*Richards*, 1980] or by the oscillatory flow induced by sea waves close to the bottom [*Blondeaux*, 1990, 2001]. Ripples are characterized by a length of the order of 10 cm and a height of the order of 1 cm. The megaripples [*Gallager et al.*, 1998] are larger bed forms, characterized by a length of the order of 1 m and a height of the order of 10 cm. Like ripples, the megaripples are generated by either steady currents or oscillatory motions induced by sea waves and tidal currents. Notwithstanding their small size, both ripples and megaripples are quite important from an engineering point of view, since they have a large influence on the damping of sea waves and on sediment transport and, hence, on the deposition and erosion processes. The largest bed forms observed in the coastal region are the sand banks and the sand waves which are generated by the interaction of the tidal currents with the sea bottom. The sand banks are long sand ridges, typically tens of meters high and tens of kilometers long, which are characterized by a spacing (crest to crest distance) of a few kilometers. The crests of sand banks are almost aligned with the major axis of the tidal ellipse, even though they usually form a small clockwise or counter-clockwise angle with the direction of the strongest tidal velocity. The recent interest on sand bank dynamics is due to the increasing demand of areas for sand extraction from the seabed and the awareness that sand banks could be a large source of sediment.

[3] The sand waves have wavelengths of the order of hundreds of meters and heights of the order of few meters and their crests are often almost orthogonal to the direction of the tidal current. As pointed out by *Besio et al.* [2006a], many human activities are confronted with the presence of sand waves. For instance, sand wave migration can represent a serious hazard to pipelines and examples can be found of free spans related to the formation and migration of sand waves [see *Santoro et al.*, 2002]. Moreover, the local water depth and consequently the navigability might be reduced by sand waves presence and migration [*Németh et al.*, 2002; *Besio et al.*, 2004], and intense dredging activities might be required [*Knaapen and Hulscher*, 2002]. Finally, objects buried into the seabed (e.g., shipwrecks, mines and containers of hazardous materials) might become exposed, forming a direct hazard, because of the appearance and/or migration of sand waves.

[4] As pointed out by *Hulscher* [1996], the mechanism which gives rise to sand waves is similar to that which originates sea ripples: a small bottom perturbation, interacting with an oscillatory motion, gives rise to steady recirculating cells. The steady velocity component close to the bottom is usually directed from the troughs towards the crests of the bottom waviness. This steady velocity compo-

[1]Department of Civil, Environmental, and Architectural Engineering, University of Genoa, Genoa, Italy.
[2]Renard Centre of Marine Geology, Ghent University, Ghent, Belgium.

0148-0227/07/2007JC004089

nent induces a sediment motion from the troughs towards the crests and hence an increase of the amplitude of the bottom waviness.

[5] The theoretical investigation of sand wave appearance forced by tide propagation has been mainly carried out by means of linear stability analyses which study the time development of arbitrary bottom perturbations of small amplitude superimposed to the flat bottom configuration. Random initial perturbations contain different spatial components which, in the linear approximation, evolve each independently of the other. Hence, a normal-mode analysis can be applied and the generic component of the perturbation can be considered. Because the horizontal directions are directions of homogeneity, the water depth h^* can be written in the form $h^*(x^*, y^*, t^*) = h_0^*[1-\epsilon A(t^*) \exp(i\alpha_x^* x^* + i\alpha_y^* y^*) + c.c.]$, where t^* is time and x^*, y^*, z^* are cartesian coordinates of a fixed reference frame with x^* and y^* lying on a horizontal plane and z^* pointing upward [*Besio et al.*, 2006b]. Hereinafter, a star denotes dimensional quantities. Moreover, $\epsilon h_0^* A(t^*)$ is the amplitude of the bottom waviness (with $\epsilon \ll 1$ and $A \sim O(1)$) and α_x^*, α_y^* indicate its wavenumbers in the homogeneous directions x^* and y^*. The time development of the perturbation of the sea bottom is controlled by mass conservation of sediment which leads to Exner equation. To integrate such an equation, a predictor for the sediment transport rate is needed and the flow must be evaluated. Different models can be used to solve the hydrodynamic problem, to evaluate the bottom shear stress and to quantify sediment transport. However, the solution procedure invariably leads to an amplitude equation for $A(t^*)$ in the form $dA(t^*)/dt^* = \Gamma^*(t^*)\, A(t^*)$, where the complex function $\Gamma^*(t^*) = \Gamma_r^*(t^*) + i\, \Gamma_i^*(t^*)$ depends on α_x^*, α_y^* and on suitable flow and sediment parameters. Since the forcing tidal flow is time periodic, the quantity Γ^* turns out to be a periodic function of time and the growth of the bottom forms is controlled by the time average $\bar{\Gamma}^*$ of Γ^*. A linear stability analysis suggests that the component of the bottom perturbation characterized by the largest value of the amplification rate (amplification rate = time averaged value of $\Gamma_r^*(t^*)$) will prevail for large times. Hence, the linear analysis predicts a specific wavelength, an orientation and a migration speed of the most unstable component of the bed perturbation which can be assumed to coincide with the appearing bed forms.

[6] The first model of sand wave appearance was formulated by *Hulscher* [1996]. Then, further contributions appeared [*Gerkema*, 2000; *Komarova and Hulscher*, 2000; *Németh et al.*, 2002; *Besio et al.*, 2003; *Besio et al.*, 2004]. The most recent model was formulated by *Besio et al.* [2006b], who studied both sand wave and sand bank appearance. To describe the hydrodynamics and the morphodynamics of shallow tidal seas, the three-dimensional model proposed by *Blondeaux and Vittori* [2005a, 2005b] was employed by *Besio et al.* [2006b] even though the local time derivative of the perturbed velocity field is included into the model equations along with the Coriolis terms. Indeed, the local acceleration terms in the momentum equations at order ϵ, neglected by *Blondeaux and Vittori* [2005a, 2005b], have the same order of magnitude of the Coriolis terms which greatly affect the orientation of the sand bank crests with respect to the direction of the major axis of the tidal ellipse [*Besio et al.*, 2006a, 2006b; *Idier and Astruc*, 2003]. Turbulence generated by tidal currents is described by using an eddy viscosity which is assumed to depend on the distance from the bottom while previous models considered a constant eddy viscosity thus being forced to introduce an empirical slip velocity at the bottom. Moreover, while previous models considered only the bed load, in the model of *Besio et al.* [2006b], sediment is supposed to move both as bed load and suspended load since, at some locations, field surveys show that large amounts of sediment are put into suspension and transported by the tidal currents.

[7] Even though some comparisons between theoretical predictions and field measurements taken at two different locations of the Dutch continental shelf are described by *Besio et al.* [2006b], to further support the validity of the model and to quantify the limits of its applicability in the parameter space, we have further tested the model predictions against field observations carried out along the continental shelf of Belgium. Field data on sediment, morphology and bathymetry are available in raster grids over the entire shelf [*Van Lancker et al.*, 2005]. Point data on tidal currents have been been described by *Mouchet* [1990]. Moreover, since the field measurements described by *Le Bot* [2001] have been carried out in a region close to that considered by *Van Lancker et al.* [2005], the model predictions have been made also for the data of *Le Bot* [2001] and the obtained results have been compared with the field measurements. Attention has been focused on the prediction of the wavelength of the bottom forms. Indeed, the capability of a stability analysis to predict the occurrence of sand waves has been already successfully tested by *Hulscher and Van den Brink* [2001] and more recently by *van der Veen et al.* [2006], who extended the model used by *Hulscher and Van den Brink* [2001] to take into account the dependency of the phenomenon on the grain size of the bottom material. However, the above works have not attempt to predict the geometrical characteristics of the bottom forms.

[8] When evaluating the performances of the theoretical model, it should be kept in mind that in the literature, quite often, comparisons between theoretical predictions and laboratory and/or field data, concerning the geometrical characteristics of the morphological patterns observed in both fluvial and coastal environments, are made considering only the order of magnitude of the results or looking at their qualitative behavior [e.g., *Trowbridge*, 1995; *Vittori et al.*, 1999; *Coco et al.*, 2000; *Komarova and Hulscher*, 2000; *Komarova and Newell*, 2000; *Gerkema*, 2000; *Calvete et al.*, 2001] and often a relative error equal to 100% is considered to be more than acceptable.

[9] The present paper is organized as follows. In the next section the main characteristics of the model of *Besio et al.* [2006b] are summarized and the definitions of the parameters of the model are given. Section 3 summarizes the available field data and provides also a brief summary of the survey procedures. Moreover, model findings and comparisons of theoretical predictions with field data are reported. Finally, section 4 is devoted to draw the conclusions of the work.

2. Theoretical Model

[10] First of all, for the sake of clearness, we summarize the theoretical approach used by *Besio et al.* [2006b] to

predict sand waves characteristics, and we list the parameters which appear in the model, referring the interested reader to *Blondeaux and Vittori* [2005a, 2005b] and *Besio et al.* [2006b] for more details.

[11] A shallow sea of small depth h^* is considered and a Cartesian coordinate system (x^*, y^*, z^*) is introduced such that the x^*-axis is horizontal and aligned with the major axis of the tidal ellipse, the y^*-axis is orthogonal to it and the z^*-axis is vertical pointing upwards and such that $z^* = 0$ describes the still water surface. The seabed is supposed to be made of a cohesionless sediment of uniform size d^* and density ρ_s^* (hereinafter a star denotes dimensional quantities). By using the *f*-plane approximation [see, e.g., *LeBlond and Mysak*, 1978], the problem of flow determination is posed by continuity and momentum equations where the Coriolis contributions related to the Earth rotation (Ω^* denotes the angular velocity of the Earth rotation and ϕ_0 is the local latitude) are taken into account because they affect the tidal current. Even though inertial effects and Coriolis terms should be taken into account in the determination of the flow induced by tide propagation over a flat bottom, they can be neglected when studying the interaction of the tidal current with a bottom waviness characterized by a length scale of the order of a few hundreds of meters as sand waves are [*Gerkema*, 2000]. Indeed, as discussed by *Besio et al.* [2006b], the characteristic horizontal length scale of tide propagation is much larger than the size of the sand waves.

[12] The flow regime is assumed to be turbulent and viscous effects are neglected. An analysis of turbulence characteristics [*Soulsby*, 1983] shows that turbulence can be assumed isotropic. Hence, the Boussinesq hypothesis can be used to model Reynolds stresses and a scalar kinematic eddy viscosity ν_T^* can be introduced.

[13] It is convenient to consider the dimensionless problem, where the mean water depth h_0^* is used as length scale, the maximum value U_0^* of the depth averaged fluid velocity during the tidal cycle is used as velocity scale and the inverse of the angular frequency of the tide ω^* is used as timescale.

[14] The dimensionless hydrodynamic problem is characterized by two main dimensionless parameters, which are denoted by $\hat{r}$ and $\hat{\delta}$, beside the values of $\Omega = \Omega^*/\omega^*$ and ϕ_0, which control the velocity profile:

$$\hat{r} = \frac{U_0^*}{\omega^* h_0^*} \quad , \quad \hat{\delta} = \frac{\sqrt{\nu_{T0}^*/\omega^*}}{h_0^*} \quad . \tag{1}$$

[15] In the definition of $\hat{\delta}$, the kinematic eddy viscosity ν_T^* is written as the product $\nu_{T0}^* \nu_T$, where the constant ν_{T0}^* is dimensional and provides the order of magnitude of the eddy viscosity while $\nu_T = \nu_T(x, y, z, t)$ is a dimensionless function (of order 1) describing the spatial and temporal variations of the turbulence structure. The parameter $\hat{r}$ is the ratio between the amplitude of horizontal fluid displacement oscillations and the local depth. Typical values of $\hat{r}$ are of the order 10^2. The parameter $\hat{\delta}$ is the ratio between the thickness of the turbulent bottom boundary layer and the local depth. A rough estimate shows that $\hat{\delta}$ is of order one. Finally, for a semidiurnal tide $\Omega \cong 0.5$ while for the diurnal tide component $\Omega \cong 1$.

[16] The time development of the bottom configuration is provided by sediment continuity equation along with a sediment transport predictor. The dimensionless parameters which characterize the morphodynamic problem are the sediment porosity p_{or}, the dimensionless sediment size d, the mobility number $\hat{\psi}_d$ and the Reynolds number R_p of sediment particles

$$d = \frac{d^*}{h_0^*} \quad ; \quad \hat{\psi}_d = \frac{(\omega^* h_0^*)^2}{(\rho_s^*/\rho^* - 1) g^* d^*} \quad ; \quad R_p = \frac{\sqrt{(\rho_s^*/\rho^* - 1) g^* d^{*3}}}{\nu} . \tag{2}$$

[17] The problem is closed once the eddy viscosity ν_T^* is given and a relationship for the sediment transport rate is provided. The eddy viscosity ν_T^* is assumed to be time-independent and given by:

$$\nu_T^* = k \frac{U_0^* h_0^*}{C} F(\xi) \quad . \tag{3}$$

[18] In (3) k is the Von Karman constant ($k = 0.4$), $F(\xi)$ describes the vertical structure of eddy viscosity which is assumed to be proportional to the time average of the local friction velocity and to the local depth h_0^*. The average friction velocity is then related to U_0^* by introducing the friction factor C, which only depends on the dimensionless roughness size $z_r = z_r^*/h_0^*$, since the Reynolds number of the flow is assumed to be large. The standard formula for steady currents can be used to evaluate C (e.g., $C = 5.75 \log_{10} (10.9\, h_0^*/z_r^*)$ [see also *Fredsøe and Deigaard*, 1992]).

[19] As pointed out in the introduction, shallow tidal seas are often covered by small scale sea ripples which are the main origin of the bottom roughness. Hence, to evaluate C, it is necessary to estimate the ripple geometry. To determine ripple characteristics, the empirical predictor proposed by *Soulsby and Whitehouse* [2005a, 2005b] has been used. This predictor allows to evaluate the height and length both of the ripples generated by the tidal currents and of those due to sea waves. Presently, it has been assumed that the former prevail on the latter and the height Δ_r^* of the ripples is evaluated by

$$\Delta_r^* = 202 d_{50}^* R_p^{-0.369} \quad . \tag{4}$$

[20] Then, following the suggestion of *Van Rijn* [1991], z_r^* is fixed equal to Δ_r^*. However, the characteristics of the ripples generated by sea waves are not too different from those which can be estimated by means of (4) [see *Soulsby and Whitehouse*, 2005a, 2005b]. Finally, the function $F(\xi)$ ($\xi = z^*/h^*$) describes the vertical structure of the eddy viscosity and it has been chosen, as suggested by *Dean* [1974], such that the eddy viscosity grows linearly with the distance from the bed, when a region close to the bottom is considered, and then decreases achieving a finite small value at the free surface ($F(\xi) = -\xi(1 + \xi)/[1 + 2A\ (\xi + 1)^2 + 3B(\xi + 1)^3]$ with $A = 1.84$ and $B = -1.56$). Therefore, ν_{T0}^* is equal to $k U_0^* h_0^* \int_{-1}^{0} F(\xi) d\xi / C$ and $\nu_T(\xi) = F(\xi) / \int_{-1}^{0} F(\xi) d\xi$. These definitions of ν_{T0}^* and ν_T have been

chosen in such a way that the depth averaged value of $\nu_T(\xi)$ is equal to one. Since ν^*_{T0} is proportional to U^*_0, for convenience, *Besio et al.* [2006b] introduced the new viscous parameter

$$\hat{\Delta} = \frac{1}{\hat{\mu}} = \frac{k\int_{-1}^{0} F(\xi)d\xi}{C} = \frac{\hat{\delta}^2}{\hat{r}} \tag{5}$$

which does not depend on the strength of the tidal current.

[21] Sediment transport is usually split into two components. The former is due to sediment moving close to the bottom (the "bed load") and the latter is due to sediment which is carried into suspension (the "suspended load"). The dimensionless bed load $(q_{Bx}, q_{By}) = (q^*_{Bx}, q^*_{By})/\sqrt{(\varrho^*_s/\varrho^* - 1)g^*(d^*)^3}$ due to the tidal current is computed by means of the relationship proposed by *Van Rijn* [1991] where the Shields stress components $(\theta_x, \theta_y) = [(\tau^*_x, \tau^*_y)/(\rho^*_s\text{-}\rho^*)\, g^*d^*]$ due to the tidal current appear:

$$(q_{Bx}, q_{By}) = \frac{0.25}{R_p^{0.2}}\left(\frac{\theta - \theta_{cr}}{\theta_{cr}}\right)^{1.5}\frac{(\theta_x, \theta_y)}{\sqrt{\theta}} \tag{6}$$

where θ is equal to $\sqrt{\theta_x^2 + \theta_y^2}$ and θ_{cr} is the critical value of the Shields parameter below which no sediment moves. Of course (q_{Bx}, q_{By}) vanish when θ is smaller than θ_{cr} and (6) can be used to evaluate the sediment transport rate only for θ larger than θ_{cr}.

[22] The dimensional shear stress components (τ^*_x, τ^*_y) can be easily evaluated by means of the constitutive law. As pointed out by *Colombini* [2004], the shear stress exerted by the fluid on the sediment moving close to the bed should be evaluated at top of the so-called bed load layer. In other words, it is the shear stress τ^*_l which is present at some distance from the bed and not the shear stress τ^*_b at the bed which should be used to estimate the bed load discharge. Due to the small thickness of the bed load layer, the difference in modulus between τ^*_l and τ^*_b is typically so small that it can be safely neglected. Nonetheless, *Colombini* [2004] showed that the spatial phase of the shear stress relative to the bed elevation, which drives the instability process, varies significantly in the neighborhood of the reference level, so that this assumption can lead to incorrect predictions of the characteristics of the bottom forms. Therefore, as in *Colombini* [2004], a new parameter is introduced in the analysis, namely the thickness of the bed load layer h^*_b. In *Colombini* [2004], the basic bed configuration is assumed to be plane and h^*_b is assumed to be proportional to the grain size

$$h^*_b = l_b d^* \quad . \tag{7}$$

[23] On the basis of experimental observations [*Sekine and Kikkawa*, 1992; *Lee and Hsu*, 1994], it turns out that l_b is an increasing function of the bed shear stress, which can be written in the form

$$l_b = 1 + 1.3\left(\frac{\theta - \theta_{cr}}{\theta_{cr}}\right)^{0.55}. \tag{8}$$

[24] However, in the present case, the bed is assumed to be covered by ripples and the thickness of the so-called bed load layer scales with the ripple height. Therefore, it has been heuristically assumed that (7) can be still applied with d^* replaced by z^*_r and l_b still provided by (8).

[25] To complete the description of the sediment transport which takes place close to the seabed, besides the contribution due to the current evaluated by means of the *Van Rijn* [1991] approach, it is necessary to account for the weak effects associated with a slow spatial variation of the bottom topography, which affect the bed load sediment transport. Assuming that the bottom slope ∇h is small, simple dimensional arguments coupled with linearization lead to the following contribution

$$(q_{Px}, q_{Py}) = -q_B \boldsymbol{G}\nabla h \tag{9}$$

where $\mathbf{G}$ is a dimensionless second order 2-D tensor and q_B is the bed load due to the current. Experimental observations of various authors [*Talmon et al.*, 1995] provide estimates for the components of $\mathbf{G}$ [*Seminara*, 1998]. In the intrinsic orthogonal coordinate system (s,n), with s aligned with the bottom stress, it turns out that:

$$G_{ss} = -\frac{\theta_c}{\mu}\frac{dq_B}{d\theta} \quad , \quad G_{sn} = G_{ns} = 0 \quad , \quad G_{nn} = -\frac{\beta q_B}{\sqrt{\theta}} \tag{10}$$

where μ is equal to the dynamic friction coefficient of the sediment and β is an empirical factor roughly about 0.5–0.6 [*Talmon et al.*, 1995]. In the present version of the model, μ has been fixed equal to 0.5 and β equal to 0.55.

[26] To evaluate the suspended sediment transport $(q_{Sx}, q_{Sy}) = (q^*_{Sx}, q^*_{Sy})/\sqrt{(\varrho^*_s/\varrho^* - 1)g^*(d^*)^3}$, a standard convection-diffusion equation for the sediment concentration $c = c(x^*, y^*, z^*, t^*)$ is solved, where the dimensionless particle fall velocity $w_s = w^*_s/\sqrt{(\varrho^*_s/\varrho^* - 1)g^*d^*}$ appears, which depends on the sediment Reynolds number R_p. Suitable boundary conditions are forced at the seabed and at the free surface. The latter states the vanishing of sediment flux normal to the free surface, while the former forces a reference concentration c_a at a distance from the seabed equal to 0.01 h^*. Following *Van Rijn* [1991]

$$c_a = 1.5\frac{d}{R_p^{0.2}}\left(\frac{\theta - \theta_{cr}}{\theta_{cr}}\right)^{3/2} \quad . \tag{11}$$

[27] Then, the suspended sediment transport (q_{Sx}, q_{Sy}) is computed as the flux of concentration over the water column and the total dimensionless sediment transport rate is evaluated as $(q_{Tx}, q_{Ty}) = (q_{Bx}, q_{By}) + (q_{Px}, q_{Py}) + (q_{Sx}, q_{Sy})$.

[28] In the analysis of the stability of the flat bottom configuration of a shallow tidal sea, small perturbations of the bottom are considered so that the bottom configuration differs from the flat one by a small (strictly infinitesimal) amount proportional to ϵ. Hence, the bottom profile can be thought to be given by the superposition of different spatial components which evolve one independently from the other. A normal mode analysis can be performed and the problem can be solved for the generic spatial component

$$\frac{h^*}{h^*_0} = 1 - \epsilon A(t)e^{i\left(\alpha_x x + \alpha_y y\right)} + c.c. + O\left(\epsilon^2\right) \tag{12}$$

where $A(t)$ is the amplitude of the generic component which is periodic in the x- and y-directions with dimensionless wavenumbers $\alpha_x = \alpha_x^* h_0^*$ and $\alpha_y = \alpha_y^* h_0^*$, respectively, and $\epsilon \ll 1$ ($x = x^*/h_0^*$, $y = y^*/h_0^*$, $t = t^*\omega^*$). The small value of ϵ allows the solution to be expanded in terms of ϵ.

[29] At the leading order of approximation, i.e., $O(\epsilon^0)$, the problem is reduced to the determination of both the flow and sediment transport induced by tide propagation over a flat seabed. Presently, at the leading order of approximation, the local flow is supposed to be dominated by the main tide constituent and the integration of the momentum equations provides the velocity profile once the value of the ratio e_{cc} between the minor and major axes of the tidal ellipse is obtained from field surveys. Let us only point out that two solutions exist: one describes a clockwise rotating tidal velocity vector, the other describes a counter-clockwise rotating tidal velocity vector. The direction of rotation of the tidal velocity depends on the propagation of the tidal wave and on its interaction with the horizontal boundaries and cannot be predicted on the basis of the model of *Besio et al.* [2006b], but it can be fixed on the basis of field surveys. Incidentally, it is worth pointing out that numerical experiments made with the present model have shown that the clockwise/counter-clockwise rotation of the tide velocity vector has no significant influence on the geometrical characteristics of the predicted sand waves. Then the hydrodynamic problem for the flow perturbations is solved by using the approach of *Blondeaux and Vittori* [2005a, 2005b] since inertial and Coriolis effects are negligible in the present context.

[30] The equation which provides the time development of the amplitude of the bottom perturbation follows from the sediment continuity equation which, at the order ϵ, reads

$$\frac{dA(T)}{dT} = \Gamma(t)A(T) \tag{13}$$

where Γ is a periodic, complex function of t which depends on the parameters of the problem. In (13), the slow morphodynamic timescale T appears

$$T = \frac{td}{(1 - p_{or})\sqrt{\hat{\psi}_d}} \quad . \tag{14}$$

[31] The solution of (13) shows that the growth or the decay of the bottom perturbation is controlled by the real part $\bar{\Gamma}_r$ of the time average $\bar{\Gamma}$ of Γ, while the imaginary part $\bar{\Gamma}_i$ is related to the migration speed of the perturbations. Because of the symmetry of the forcing flow, no migration of the bottom forms is expected and indeed $\bar{\Gamma}_i$ vanishes. The remaining periodic parts of Γ, given by $(\Gamma - \bar{\Gamma})$, describe the oscillations of the bottom forms around their average configuration. These oscillations turn out to be quite small since the tide period is much smaller than the morphodynamic timescale.

3. Comparison Between Theoretical Predictions and Field Measurements

3.1. Field Data From the Belgian Continental Shelf

[32] The Belgian territorial waters (approximately from 51,1° to 51,7°N and from 2,25° to 3,50°E) occupy about 300 km^2 in the southern part of the North Sea. The Belgian Continental Shelf is typically very shallow, partly due to the presence of sandbanks, with water depths ranging from 5 to 55 m MLLWS (Mean Lowest Low Water at Spring, see Figure 1).

[33] The area is subject to a semidiurnal macrotidal regime, and the amplitude of the semidiurnal constituent depends on the exact location, ranging between values of 3 m for neap tides and 4.5 to 5 m for spring tides.

[34] In the present study, to estimate the tidal currents, we have used the measurements carried out at 8 locations [*Mouchet*, 1990], namely i) Kwintebank (51°21′N, 2°41′E), ii) Nieuwpoortbank (51°10′N, 2°35′E), iii) Trapegeer (51°08′N, 2°34′E), iv) Thorntonbank (51°34′N, 2°59′E), v) Wandelaar (51°23′N, 3°03′E), vi) Westhinder (51°23′N, 2°36′E), vii) Akkaert NE (51°27′N, 2°59′E), viii) Akkaert Noord (51°23′N, 2°37′E) (see Figure 1). Then, the characteristics of the tidal constituents (ellipse orientation, ellipticity…) have been computed on the basis of the available data. At these locations, the harmonical analysis shows that the semidiurnal component is the dominant one with maximum velocities ranging from 54 to 70 cm/s. The tidal currents were measured at different water depths but they have been converted to depth averaged velocities by using the velocity profile predicted by the model and using an iterative procedure.

[35] Sediment characteristics have been obtained from a digital terrain model (250 × 250 m) of the median grain-size of the sand fraction [*Verfaillie et al.*, 2006]. The data originated from the sedisurf@database (Ghent University, Renard Centre of Marine Geology) contain about 7000 sampling points. The gridding has been performed using the bathymetric gradient as secondary variable allowing a more realistic modeling of the grain-size distributions [*Verfaillie et al.*, 2006].

[36] On the Belgian Continental Shelf, the nature and differentiation of the superficial sediments are related to the unique configuration of the sandbank-swale system and to the interaction of the current with the large-scale morphological patterns which is responsible of a hydraulic sorting of the sediment. The sand fraction (0.063 to 2 mm) preferentially takes part in the process of sandbank formation whilst the coarser sands (>2mm) and the silt-clay fraction (<0.063 mm) are found in the swales. Moreover, the superficial sediments coarsen in the offshore direction. Very fine to fine sands dominate the near coastal area whilst in the offshore area, medium sand grains up to 400–500 μm can be found (Figure 2). Usually, coarser sediments are associated with shell hash admixtures.

[37] The values of the water depths have been derived from a bathymetry digital terrain model (250 × 250 m) compiled at Ghent University on the basis of the hydrographic data of the Flemish Hydrography, Maritime Services (Ministry of the Flemish Community [*Van Lancker et al.*, 2005]). The data set consists of tidally corrected single-beam measurements.

[38] The occurrence and dimensions of sand waves have been derived from a morphological map compiled at Ghent University [*Van Lancker et al.*, 2005]. The information has been gathered from high-resolution acoustic data (multi-beam, side-scan sonar). The wavelengths of the bottom forms have been determined along profiles perpendicular

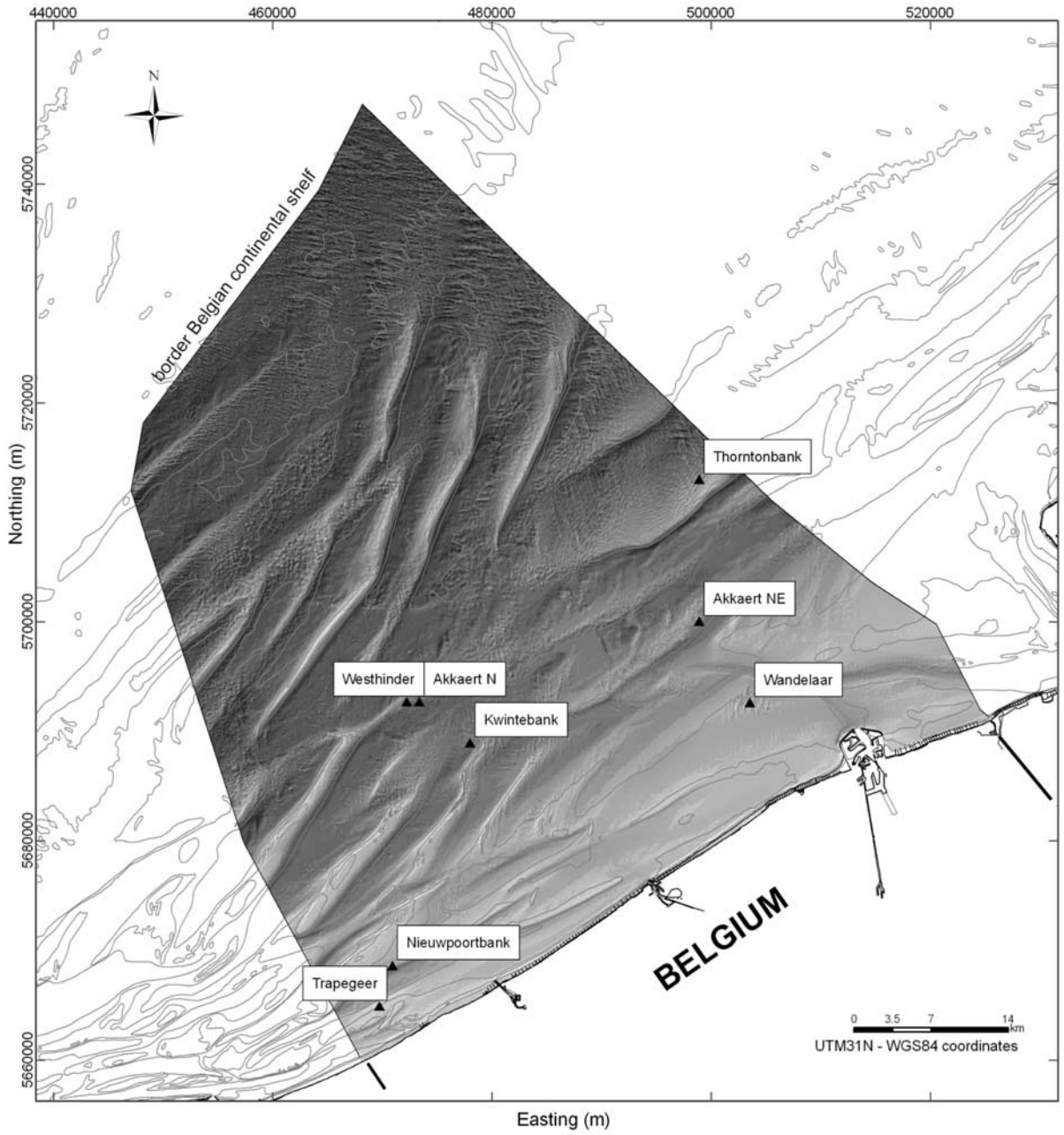

Figure 1. Bathymetry digital terrain model (DTM) of the Belgian Continental Shelf [*Van Lancker et al.*, 2005]. The current meter locations are indicated. The DTM provides a rough estimate of the presence of sand waves.

to the main strike of the sand waves. The range of values is given in Table 3.

[39] Sand waves, 2 to 4 m in height, are generally present where sandbanks occur, except for the Coastal Banks. In the coastal zone, patches of sand waves do occur where a coarse sediment is present. To the north of the Belgian Continental Shelf, fields of sand waves characterize the seabed with heights that are often more than 6 m. The sand waves occur both along the flanks of the sand banks and in the swales and over the flat beds. Over the Belgian Continental Shelf, sand wave wavelengths vary considerably, ranging from 100 to 800 m.

[40] The model has been run for values of the parameters chosen to reproduce the eight locations where tidal current data are available. Therefore, both small (6 m) and relatively large (28 m) water depths are considered and the sediment size ranges from 0.22 mm to 0.38 mm. Since detailed information on the size of the small scale bottom forms (ripples) were not available, the characteristics of ripples which control the roughness of the bottom have been estimated on the basis of the empirical predictor of *Soulsby and Whitehouse* [2005a, 2005b]. In particular, the model has been run for the values of the parameters given in Table 1.

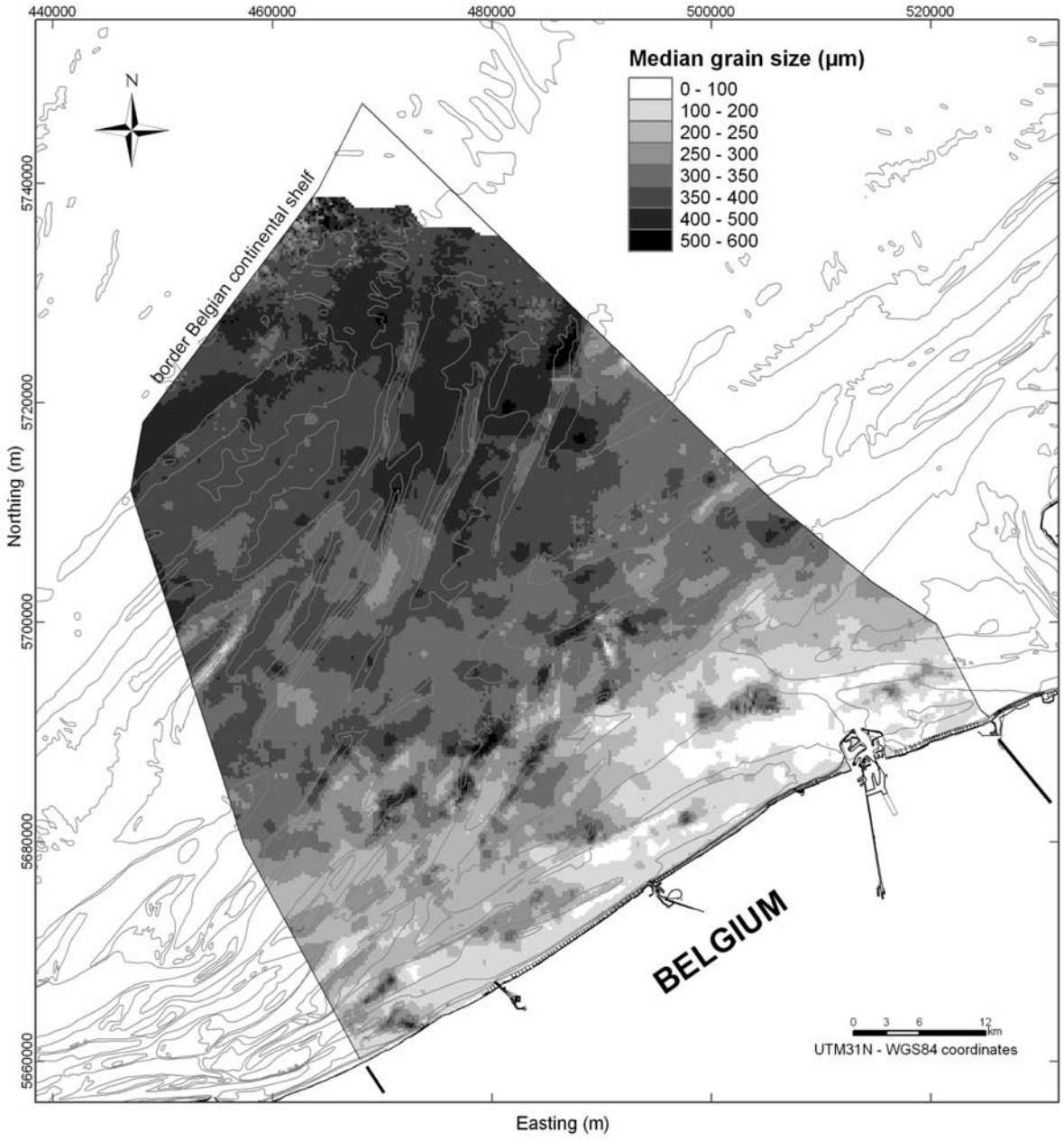

Figure 2. Median grain size of the sand fraction along the Belgian Continental Shelf [*Verfaillie et al.*, 2006].

Table 1. Values of Dimensional and Dimensionless Parameters Used in the Model Runs for the Different Locations on the Belgian Continental Shelf[a]

	Parameters									
Site	h [m]	U_0 [m/s]	e_{cc} [-]	d_{50} [mm]	$z_r \cdot 10^4$	$\hat{\mu}$	$\hat{r}$	$\hat{\Psi}_d$	R_p	$d \cdot 10^5$
Kwintebank	23.8	0.52	0.27	0.35	8.96	379.85	155.29	$2.04\ 10^{-3}$	26.16	1.48
Nieupoortbank	10.0	0.49	0.23	0.24	18.15	351.36	347.27	$5.18\ 10^{-4}$	15.03	2.44
Trapegeer	6.3	0.47	0.12	0.21	27.06	335.22	531.8	$2.37\ 10^{-4}$	12	3.35
Thorntonbank	21.5	0.46	0.34	0.33	9.62	376.99	151.73	$1.79\ 10^{-3}$	23.64	1.53
Wandelaar	11.8	0.59	0.48	0.30	16.73	354.64	306.91	$5.97\ 10^{-4}$	20.08	2.51
Westhinder	21.5	0.70	0.17	0.34	9.74	376.48	231.6	$1.74\ 10^{-3}$	24.61	1.57
Akkaert NE	16.3	0.64	0.35	0.32	12.57	366.2	279.18	$1.05\ 10^{-3}$	22.79	1.97
Akkaert N	24.1	0.62	0.22	0.31	8.33	382.8	182.97	$2.40\ 10^{-3}$	21.11	1.27

[a]The parameter e_{cc} is defined as the ratio between the minor and major axes of the tidal ellipse.

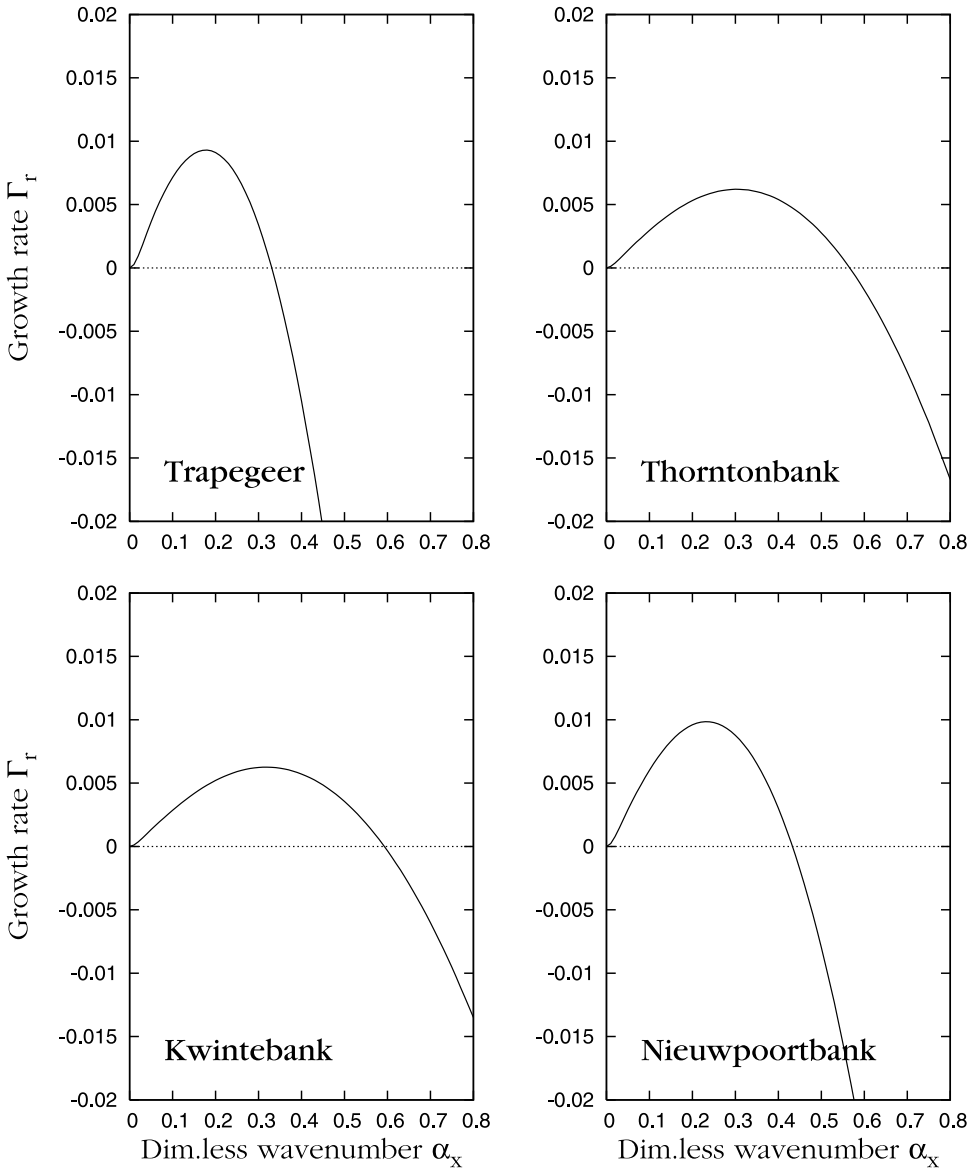

Figure 3. The growth rate $\bar{\Gamma}_r$ of the bottom perturbations plotted versus the dimensionless wavenumber α_x. The x-axis is supposed to be aligned with the major axis of the tidal ellipse. The name of the location is that appearing in Figure 1.

[41] Since the maximum of the amplification rate takes place always for $\alpha_y = 0$, in Figures 3 and 4 the amplification rate $\bar{\Gamma}_r$ is plotted as function of α_x. A maximum of $\bar{\Gamma}_r$ is present for all the locations presently considered and, according to the linear stability analysis, this maximum corresponds to the bottom perturbation the growth of which gives rise to sand waves. Hence, the dimensional wavelength of the bottom forms can be computed once the local water depth is fixed. Figure 7 shows that the predicted values are in fair agreement with the observed values. Moreover, the knowledge of the value of the amplification rate Γ_r allows an estimate of the response time of the bottom forms to the external forcing flow. Indeed, the dimensionless response time is proportional to Γ_r^{-1}. Then, taking into account the definition of the morphodynamic dimensionless timescale T (14), it turns out that the dimensional response time T_r^* is

$$T_r^* = \frac{(1 - p_{or})\sqrt{\hat{\psi}_d}}{\Gamma_r \, d\omega^*} \quad . \tag{15}$$

[42] Therefore, while the sand waves observed at Thorntonbank are characterized by values of T_r^* of $O(10^4)$ days, the sand waves observed at Westhinder are characterized by values of T_r^* of $O(10^3)$ days. These values are in agreement with those described by *Katoh et al.* [1998] and determined by *Knaapen and Hulscher* [2002], who showed that sand waves tend to regain their shape and amplitude after dredging and toping off. In particular, *Katoh et al.* [1998] showed that sand waves regenerate in several years time.

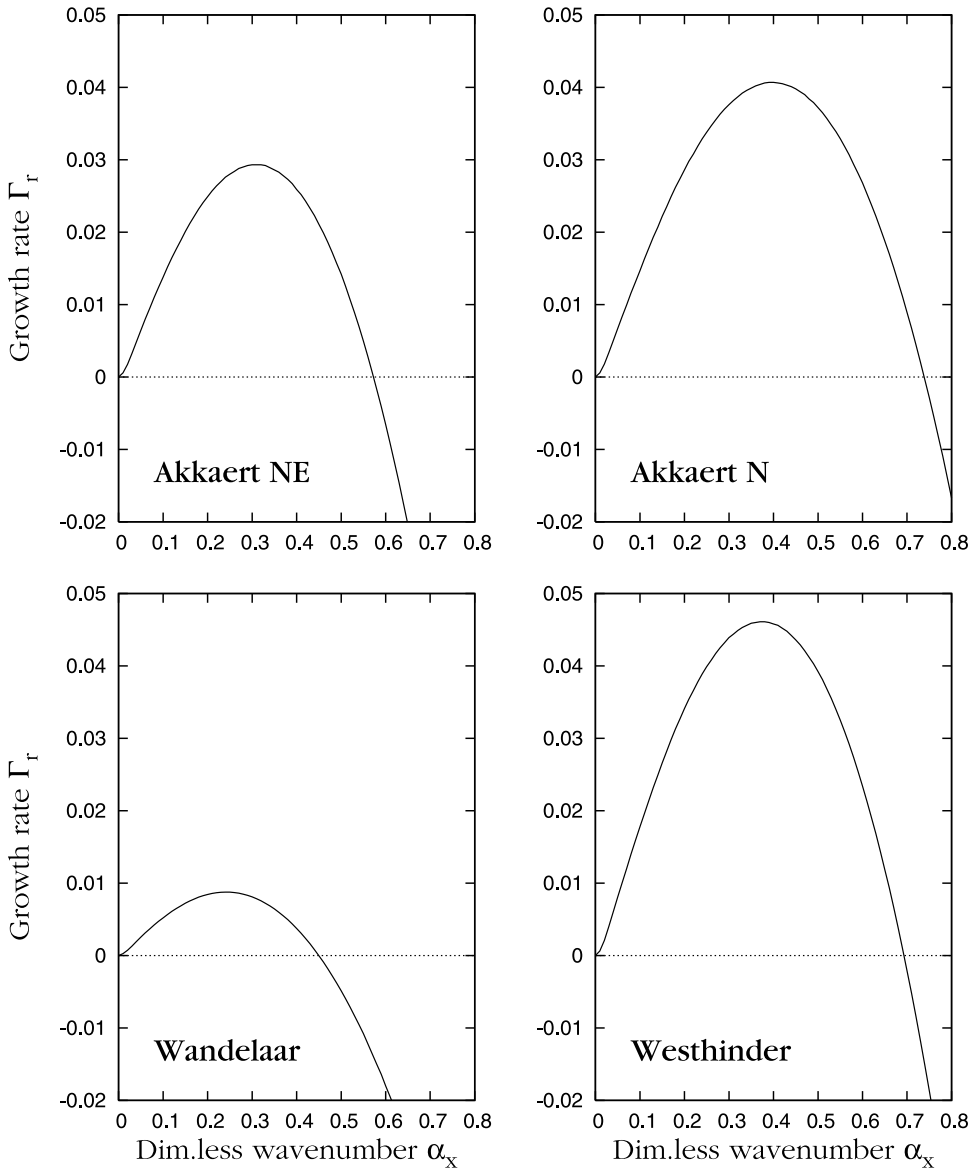

Figure 4. The growth rate $\bar{\Gamma}_r$ of the bottom perturbations plotted versus the dimensionless wavenumber α_x. The x-axis is supposed to be aligned with the major axis of the tidal ellipse. The name of the location is that appearing in Figure 1.

3.2. Field Data From the Calais-Dover Channel

[43] *Le Bot and Trenteseaux* [2004] studied a sand wave field in the Strait of Calais-Dover (Southern North Sea) at the convergence of the South Falls and Sandettie sand banks (51°05′N, 01°39′E) (see Figure 5). The area is subject to a semidiurnal macrotidal regime and the tidal range is about 3.5 m for neap tides and 6.5 m for spring tides. Surface tidal current measurements are described by *Le Bot and Trenteseaux* [2004]. The measurements were carried out during 9 days at 51°06,15′N and 01°38,14′E. The currents reach 75 to 105 cm/s in neap tides and 140 to 185 cm/s in spring tides. The velocity shows an asymmetry which is enhanced by the strait configuration. A harmonical decomposition was made by *Le Bot and Trenteseaux* [2004] and the results have been used as input for the model. Since the model uses the depth averaged value of the tidal current as input parameter, the data on the surface velocity have been converted to depth averaged velocities by assuming that the velocity profile is that predicted by the model. The tidal current turns out to be dominated by the semidiurnal constituent with an amplitude of the velocity oscillations equal to 0.94 m/s and a ratio between the minor and the major axis of the tidal ellipse equal to 0.061. Even though significant residual currents are present, which cause the migration of the bed forms, they are usually supposed to exert a negligible influence on the process of sand wave formation [*Hulscher*, 1996; *Gerkema*, 2000; *Besio et al.*, 2006b]. Hence, the steady velocity component has not been taken into account in the model.

[44] In the site, the sediment suffers from a strong heterogeneity. In fact the mean value d_{50} of the grain size is estimated to be 0.315 mm but in the SE sector a bottom composed of pebbles mixed with a little sand is present. Indeed, the acceleration of the tidal current approaching the

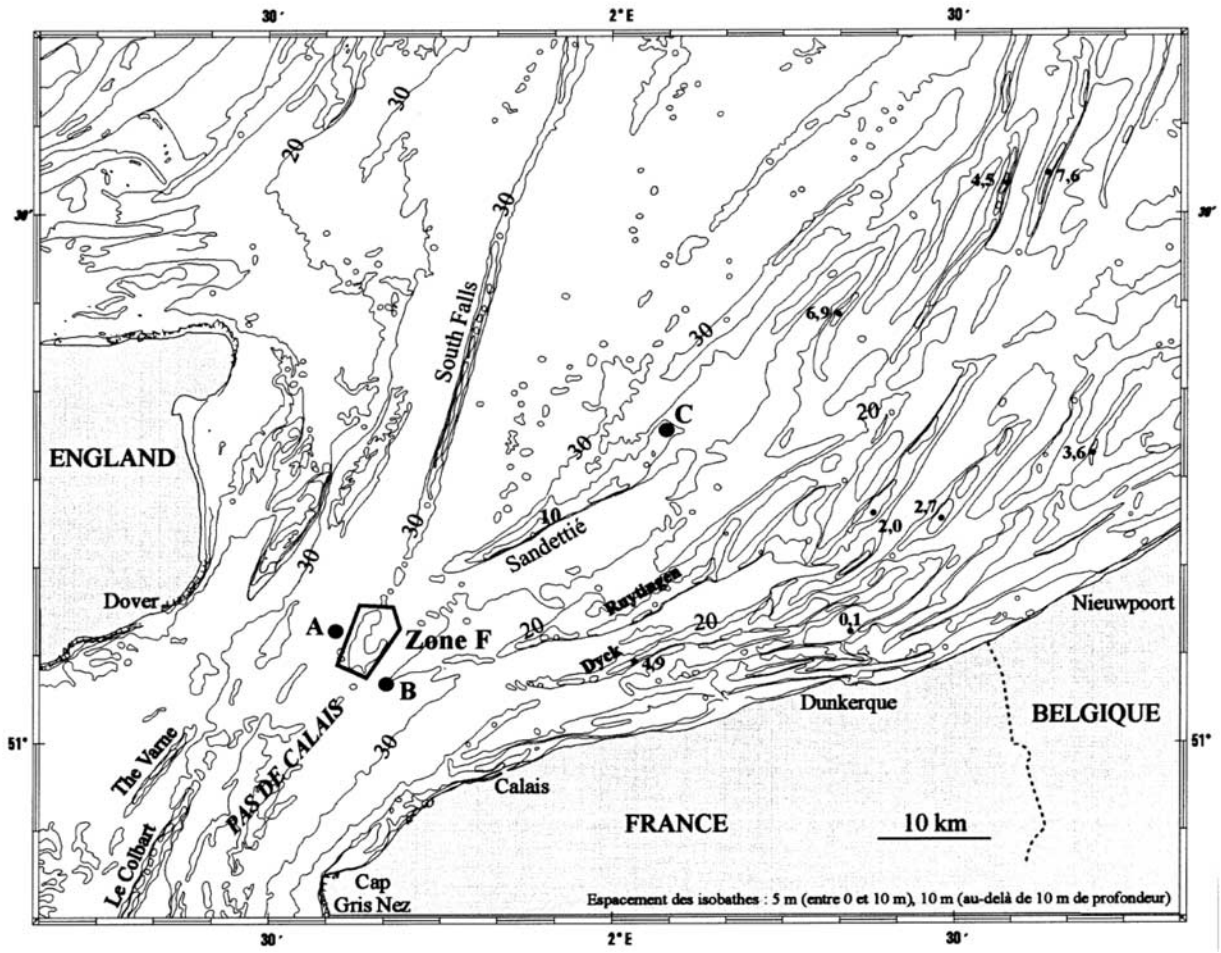

Figure 5. Bathymetric chart of the southern North Sea and the Dover Strait. Location of study area (zone F). Adapted from *Le Bot et al.* [2000].

strait prevents the deposition and preservation of sand, leading to a pebble pavement mantled with a series of sand bed forms, mainly represented by sand waves [*Le Bot and Trenteseaux*, 2004].

[45] Moreover, a grain sorting process, which is induced by the presence of large scale bed forms, leads coarse sand (2.0–2.5 mm) to pile up at the upstream slope of the large scale bed forms while in the remaining parts of the bottom forms the sediment is smaller (upstream is here referred to the net migration direction of the bottom forms). Some parts of the surveyed area are covered with ripples and megaripples. In particular in the NW sector megaripples with an height ranging between 20 to 40 cm and a wavelength equal to 3 to 8 m are present along with ripples with average height and length equal to 2 cm and 15 cm, respectively. The sea floor gently slopes from 32 m (NW) to 39 m (SE) and is covered by numerous sand waves with wavelengths ranging from 350–750 m.

[46] Presently, following *Le Bot and Trenteseaux* [2004], to run the model the site has been divided into two homogeneous parts (NW sector and SE sector) with averaged water depths of 33 m and 36 m, respectively. The analysis of *Le Bot and Trenteseaux* [2004] shows that in the NW sector the sand waves have an average wavelength of about 350 m while in the SE sector the wavelength is about 550 m.

[47] Therefore, the model has been run with the values of the parameters reported in Table 2. The amplification rate $\bar{\Gamma}_r$ is plotted as function of α_x in Figure 6 for the NW and SE sectors, respectively. A maximum of the amplification rate is present for α_x equal to 0.385 and 0.405, respectively. Taking into account the local water depth, the predicted

Table 2. Values of Dimensional and Dimensionless Parameters Used in the Model Runs for the Calais-Dover Channel[a]

	Parameters									
Site	h [m]	U_0 [m/s]	e_{cc} [-]	d_{50} [mm]	$z_r \cdot 10^4$	$\hat{\mu}$	$\hat{r}$	$\hat{\Psi}_d$	R_p	$d \cdot 10^6$
Calais NW	33.0	0.85	0.06	0.315	6.15	395.05	182.62	$4.39\ 10^{-3}$	22.05	9.55
Calais SE	36.0	0.85	0.06	0.315	$5.64\ 10^{-4}$	398.57	167.4	$5.22\ 10^{-3}$	22.05	8.75

[a]The parameter e_{cc} is defined as the ratio between the minor and major axes of the tidal ellipse.

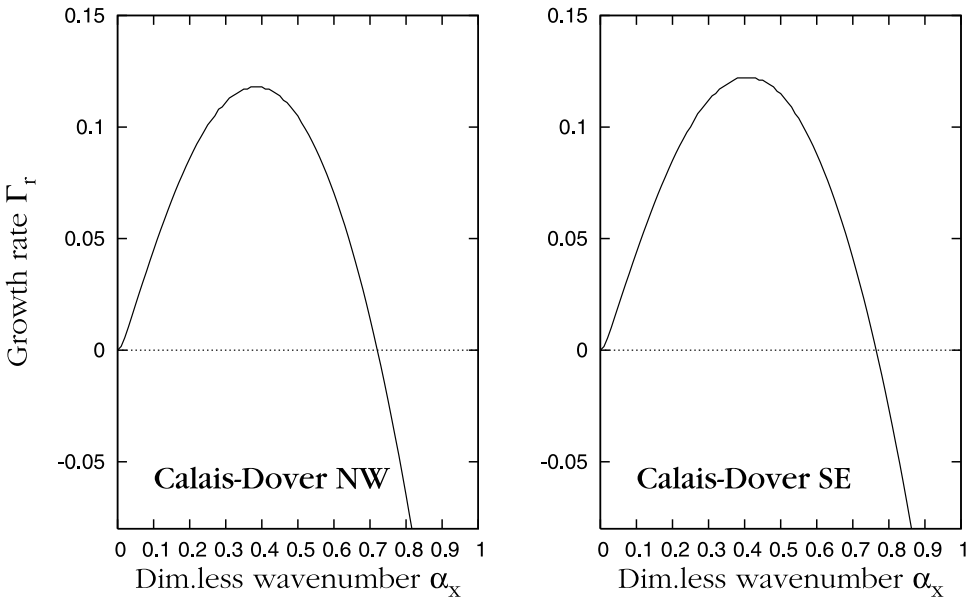

Figure 6. The growth rate $\bar{\Gamma}_r$ of the bottom perturbations plotted versus the dimensionless wavenumber α_x. The x-axis is supposed to be aligned with the major axis of the tidal ellipse. The name of the location is that defined in the text.

wavelengths of the sand waves are about 538 and 587 meters, respectively. These values are in fair agreement with the observed values (see Figure 7 and Table 3).

4. Conclusions

[48] The main results of the work are summarized in Figure 7 and Table 3 which show the observed wavenumbers along with the predicted values for all the cases considered in the present work. The general agreement is good. Indeed, as already pointed out in the introduction, in the literature, comparisons between theoretical predictions and field data are often made considering the order of magnitude of the results or looking at their qualitative behavior [e.g., *Trowbridge*, 1995; *Blondeaux*, 1990; *Vittori et al.*, 1999; *Coco et al.*, 2000; *Komarova and Hulscher*, 2000; *Komarova and Newell*, 2000; *Gerkema*, 2000; *Calvete et al.*, 2001] and a relative error equal to 100% is considered to be more than acceptable.

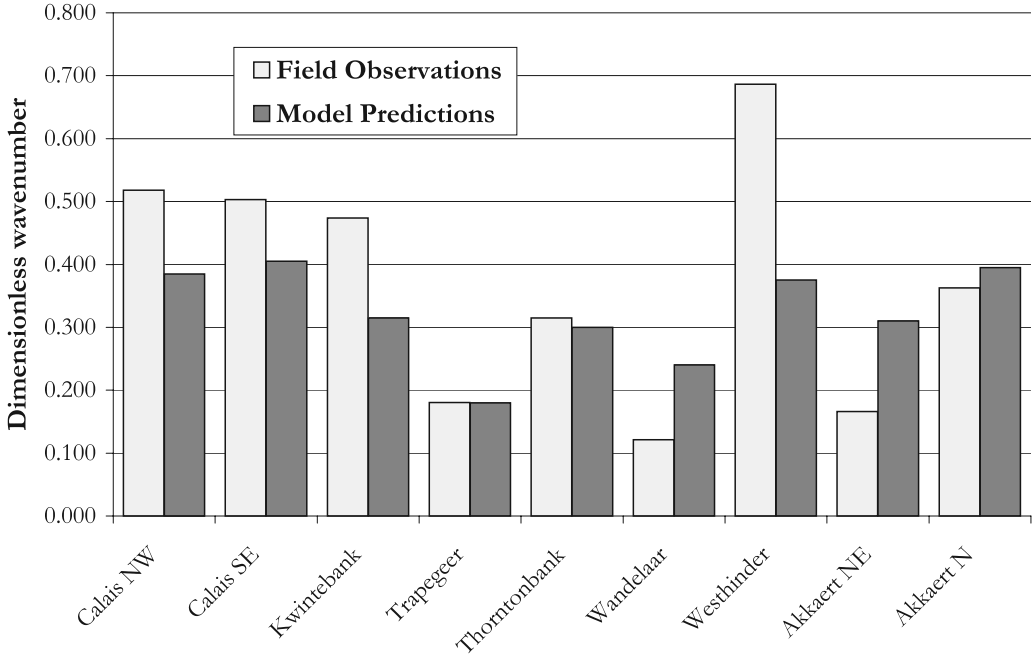

Figure 7. Dimensionless wavenumber of the bottom forms. Comparison between field observations and model results for different locations on the Belgian Continental Shelf.

Table 3. Values of the Dimensionless Wavenumbers and Dimensional Wavelengths Predicted by the Model (α_p, L_p^*) and Provided by Field Surveys (α_o, L_o^*)

	Wavenumbers and Wavelengths				
Site	α_p [-]	α_o [-]	L_p^* [m]	Mean L_o^* [m]	Min-Max L_o^* [m]
Kwintebank	0.315	0.474	475	316	240–440
Trapegeer	0.180	0.180	219	218	—
Thorntonbank	0.300	0.315	451	430	350–520
Wandelaar	0.240	0.121	309	610	437–800
Westhinder	0.375	0.687	361	197	—
Akkaert NE	0.310	0.166	331	617	400–860
Akkaert N	0.395	0.362	383	417	330–540
Calais NW	0.385	0.518	539	400	—
Calais SE	0.405	0.503	559	450	—

[49] As such, the present investigation confirms the validity of the morphodynamic model described by *Besio et al.* [2006b] aimed at predicting the formation of sand waves. Even though the data described by Stride (1982) indicate that the whole continental shelf of Belgium is covered with sand waves, field surveys have shown numerous locations where the seabed is devoid of sand waves. These areas are mainly located in the coastal zone and in the swales where the Quaternary cover is minimal. Also, the more detailed data summarized by *Hulscher and Van den Brink* [2001] and *van der Veen et al.* [2006] show the existence of spots where sand waves are absent. Even though no accurate measurements of the tide current were available to us at these locations, an attempt to apply the model was made using values of the current interpolated on the basis of the data of the nearest current-meters. The model predictions indicate the presence of sand waves. On the other hand, the present model predicts a flat bed in the north part of the North Sea where *Stride* [1982], *Hulscher and Van den Brink* [2001] and *van der Veen et al.* [2006] agree to indicate the absence of sand waves. Hence, it is possible to conclude that only the availability of accurate data can allow the prediction of the local morphology in a peculiar site where the local characteristics differ from those of the surrounding area.

[50] **Acknowledgments.** The authors thank the Italian Ministry of Education, University and Research, for the financial support provided by means of the research project "Cave sottomarine e ripascimenti: modellazione morfologica e applicazioni." Thanks are also due to S. Le Bot who gave us the reprints of the papers describing the field data of the Calais-Dover Strait. The youngest author (J.C.) acknowledges the financial support provided through the FLUBIO project of the European Union. The multibeam data presented have been acquired by FPS Economy, SMEs, Self-employed and Energy, Marine Sand Fund (RV Belgica Kongsberg-Simrad EM1002).

References

Allen, J. R. L. (1984), *Development in Sedimentology*, vols. 1 and 2, Elsevier, Amsterdam.

Besio, G., P. Blondeaux, and P. Frisina (2003), A note on tidally generated sand waves, *J. Fluid Mech.*, *485*, 171–190.

Besio, G., P. Blondeaux, M. Brocchini, and G. Vittori (2004), On the modeling of sand wave migration, *J. Geophys. Res.*, *109*, C04018, doi:10.1029/2002JC001622.

Besio, G., P. Blondeaux, M. Brocchini, S. J. M. H. Hulscher, D. Idier, M. A. F. Knaapen, A. A. Németh, P. C. Roos, and G. Vittori (2006a), The morphodynamics of tidal sand waves: A model overview, *Coastal Eng*, in press.

Besio, G., P. Blondeaux, and G. Vittori (2006b), On the formation of sand waves and sand banks, *J. Fluid Mech.*, *557*, 1–27.

Blondeaux, P. (1990), Sand ripples under sea waves: Part I. Ripple formation, *J. Fluid Mech.*, *218*, 1–17.

Blondeaux, P. (2001), Mechanics of coastal forms, *Ann. Rev. Fluid Mech.*, *33*, 339–370.

Blondeaux, P., and G. Vittori (2005a), Flow and sediment transport induced by tide propagation: 1. The flat bottom case, *J. Geophys. Res.*, *110*, C07020, doi:10.1029/2004JC002532.

Blondeaux, P., and G. Vittori (2005b), Flow and sediment transport induced by tide propagation: 2. The wavy bottom case, *J. Geophys. Res.*, *110*, C08003, doi:10.1029/2004JC002545.

Calvete, D., A. Falques, H. E. De Swart, and M. Walgreen (2001), Modelling the formation of shoreface-connected sand ridges on storm-dominated inner shelves, *J. Fluid Mech.*, *441*, 169–193.

Coco, G., D. A. Huntley, and T. J. O'Hare (2000), Investigation of a self-organized model for beach cusp formation and development, *J. Geophys. Res.*, *105*(C9), 21,991–22,002.

Colombini, M. (2004), Revisiting the linear theory of sand dune formation, *J. Fluid Mech.*, *502*, 1–16.

Dean, R. B. (1974), *AERO Rep. 74-11*, Imperial Coll., London.

Fredsøe, J., and R. Deigaard (1992), *Mechanics of Coastal Sediment Transport*, *Adv. Ser. Ocean Eng.*, xviii + 369 pp., World Sci., Singapore.

Gallager, E. L., S. Elgar, and E. B. Thornton (1998), Observations and predictions of megaripple migration in a natural surf zone, *Nature*, *394*, 165–168.

Gerkema, T. (2000), A linear stability analysis of tidally generated sand waves, *J. Fluid Mech.*, *417*, 303–322.

Hulscher, S. J. M. H. (1996), Tidal-induced large-scale regular bed form patterns in a three-dimensional shallow water model, *J. Geophys. Res.*, *101*(C9), 20,727–20,744.

Hulscher, S. J. M. H., and G. M. Van den Brink (2001), Comparison between predicted and observed sand waves and sand banks in the North Sea, *J. Geophys. Res.*, *106*(C5), 9327–9338.

Idier, D., and D. Astruc (2003), Analytical and numerical modeling of sandbanks dynamics, *J. Geophys. Res.*, *108*(C3), 3060, doi:10.1029/2001JC001205.

Katoh, K., H. Kume, K. Kuroki, and J. Hasegawa (1998), The development of sand waves and the maintenance of navigation channels in the Bisanteto Sea, in *Proceedings of International Conference on Coastal Engineering*, pp. 3490–3502, Am. Soc. of Civ. Eng., Reston, Va.

Knaapen, M. A. F., and S. J. M. H. Hulscher (2002), Regeneration of sand waves after dredging, *Coastal Eng.*, *46*, 277–289.

Komarova, N. L., and S. J. M. H. Hulscher (2000), Linear instability mechanism for sand wave formation, *J. Fluid Mech.*, *413*, 219–246.

Komarova, N. L., and A. C. Newell (2000), Nonlinear dynamics of sand banks and sand waves, *J. Fluid Mech.*, *415*, 285–312.

LeBlond, P. H., and L. A. Mysak (1978), *Waves in the Ocean*, xiv + 602 pp., Elsevier, Sci., Amsterdam.

Le Bot, S. (2001), Morphodynamics of submarine dunes under the influence of tides and storms, Ph.D. thesis, 272 pp., Univ. of Lille 1, France.

Le Bot, S., and A. Trenteseaux (2004), Types of internal structure and external morphology of submarine dunes under the influence of tidal and wind-driven processes (Dover Strait, Northern France), *Mar. Geol.*, *211*, 143–168.

Le Bot, S., A. Trentesaux, T. Garlan, S. Berne, and H. Chamley (2000), Influence des tempetes sur la mobilite des dunes tidales dans le detroit du Pas-de-Calais, *Oceanol. Acta*, *23*(2), 129–141.

Lee, H. Y., and I. S. Hsu (1994), Investigation of saltating particle motion, *J. Hydraul. Eng.*, *120*, 831–845.

Mouchet, A. (1990), Analysis of tidal elevations and currents along the Belgian coast, *MUMM - BH/88/29*, 52 pp., Univ. of Liege, Liege, Belgium.

Németh, A. A., S. J. M. H. Hulscher, and H. J. de Vriend (2002), Modelling sand wave migration in shallow shelf seas, *Cont. Shelf Res.*, *22*, 2795–2806.

Richards, K. J. (1980), The formation of ripples and dunes on an erodible bed, *J. Fluid Mech.*, *99*, 597–618.

Santoro, V. C., E. Amore, E. Cavallaro, L. Cozzo, and E. Foti (2002), Sand waves in the Messina Strait, Italy, *J. Coastal Res.*, *36*, 640–653.

Sekine, M., and H. Kikkawa (1992), Mechanics of saltating grains, *J. Hydraul. Eng.*, *118*, 536–558.

Seminara, G. (1998), Stability and morphodynamics, *Meccanica*, *33*, 59–99.

Sleath, J. F. A. (1984), *Seabed Mechanics*, xv + 335 pp., John Wiley, Hoboken, N. J.

Soulsby, R. L. (1983), The bottom boundary layer of shelf seas, in *Physical Oceanography of Coastal and Shelf Seas*, edited by B. Johns, pp. 189–266, Elsevier, Amsterdam.

Soulsby, R. L., and R. J. S. Whitehouse (2005a), Prediction of ripples properties in shelf seas: Mark 1 predictor, *Rep. TR 150*, HR Wallingford Ltd, Wallingford, UK.

Stride, A. H. (1982), *Offshore Tidal Sands*, xi + 222 pp., Chapman and Hall, New York.

Soulsby, R. L., and R. J. S. Whitehouse (2005b), Prediction of ripples properties in shelf seas: Mark 2 Predictor for time evolution, *Rep. TR 154*, HR Wallingford Ltd, Wallingford, UK.

Talmon, A. M., N. Struiksma, and M. C. L. M. Van Mierlo (1995), Laboratory measurements of the direction of sediment transport on transverse alluvial-bed slopes, *J. Hydraul. Res.*, *33*, 495–517.

Trowbridge, J. H. (1995), A mechanism for the formation and maintenance of shore-oblique sand ridges on storm-dominated shelves, *J. Geophys. Res.*, *100*(C8), 16,071–16,086.

van der Veen, H. H., S. J. M. H. Hulscher, and M. A. F. Knaapen (2006), Grain size dependency in the occurrence of sand waves, *Ocean Dyn.*, *56*, 228–234.

Van Lancker, V., et al. (2005), Management, research and budgeting of aggregates in shelf seas related to end-users (MAREBASSE), *Sci. Rep. Year 3*, 144 pp., Belgian Sci. Policy, Brussels.

Van Rijn, L. C. (1991), Sediment transport in combined waves and currents, in *Proceedings of Euromech 262*, Balkema, A. A., Brookfield, Vt.

Verfaillie, E., V. Van Lancker, and M. Van Meirvenne (2006), Multivariate geostatistics for the predictive modelling of the surficial sand distribution in shelf seas, *Cont. Shelf Res.*, *26*(19), 2454–2468.

Vittori, G., H. E. De Swart, and P. Blondeaux (1999), Crescentic bed forms in the nearshore region, *J. Fluid Mech.*, *381*, 271–303.

G. Besio, P. Blondeaux, J. Cherlet, and G. Vittori, Department of Civil, Environmental, and Architectural Engineering, University of Genova, Via Montallegro 1, 16145 Genova, Italy. (giospud@dicat.unige.it)

V. van Lancker and E. Verfaillie, Renard Centre of Marine Geology, Ghent University, Krijgslaan 281, S8 - B-9000 Gent, Belgium.